Spatial segregation of neuronal calcium signals encodes different forms of LTP in rat hippocampus

Clarke R. Raymond and Stephen J. Redman

Division of Neuroscience, John Curtin School of Medical Research, Australian National University, Canberra, ACT 0200, Australia

Calcium regulates numerous processes in the brain. How one signal can coordinate so many diverse actions, even within the same neurone, is the subject of intense investigation. Here we have used two-photon calcium imaging to determine the mechanism that enables calcium to selectively and appropriately induce different forms of long-term potentiation (LTP) in rat hippocampus. Short-lasting LTP (LTP 1) required activation of ryanodine receptors (RyRs), which selectively increased calcium in synaptic spines. LTP of intermediate duration (LTP 2) was dependent on activation of inositol 1,4,5-trisphosphate (IP_3) receptors (IP_3Rs) and subsequent calcium release specifically in dendrites. Long-lasting LTP (LTP 3) was selectively dependent on L-type voltage-dependent calcium channels (L-VDCCs), which generated somatic calcium influx. Activation of NMDA receptors was necessary, but not sufficient, for the generation of appropriate calcium signals in spines and dendrites, and the induction of LTP 1 and LTP 2. These results suggest that the selective induction of different forms of LTP is achieved via spatial segregation of functionally distinct calcium signals.

(Received 27 September 2005; accepted after revision 4 November 2005; first published online 10 November 2005)
Corresponding author C. R. Raymond: Division of Neuroscience, John Curtin School of Medical Research, Australian National University, Canberra, ACT 0200, Australia. Email: clarke.raymond@anu.edu.au

The calcium ion is one of the most pervasive second-messengers in the brain, implicated in a diverse array of cellular processes. How does a promiscuous second-messenger like Ca^{2+} achieve signalling specificity? One idea that has received considerable attention recently is spatial compartmentalization (Delmas & Brown, 2002; Augustine *et al.* 2003), whereby an increase in Ca^{2+} in a specific location activates a specific effector mechanism. While the evidence for spatial heterogeneity in neuronal Ca^{2+} signalling is mounting (Augustine *et al.* 2003), few examples of its functional significance have been identified.

One Ca^{2+}-sensitive phenomenon of particular interest is long-term potentiation (LTP), which is widely accepted as a learning and memory mechanism in the brain (Martin *et al.* 2000; Lynch, 2004). It is well known that the induction of LTP in CA1 pyramidal neurones depends largely on activation of postsynaptic *N*-methyl-D-aspartate receptors (NMDARs) and subsequent influx of Ca^{2+} (Bliss & Collingridge, 1993). However, it is less clear whether NMDAR-mediated Ca^{2+} influx *per se* is sufficient for LTP induction, or whether this Ca^{2+} is augmented by other sources.

An important feature of LTP that is often overlooked is that it is not a unitary phenomenon. In area CA1 of the hippocampus, there is good evidence that at least three forms of LTP coexist in the one synaptic pathway. We favour the LTP 1, 2 and 3 nomenclature (Racine *et al.* 1983; Abraham & Otani, 1991; Bliss & Collingridge, 1993; Raymond & Redman, 2002), but they have also been termed early-, intermediate- and late-LTP. These forms of LTP differ in their persistence and their reliance on different biochemical maintenance mechanisms. LTP 1 is short lasting and dependent on post-translational modifications of key synaptic proteins (Lovinger *et al.* 1987; Malinow *et al.* 1988). LTP 2 is of intermediate duration and requires new protein synthesis, but not gene transcription (Otani *et al.* 1989; Raymond *et al.* 2000; Kelleher *et al.* 2004*a*). LTP 3 is very durable, perhaps even permanent, and depends on gene transcription (Nguyen *et al.* 1994; Frey *et al.* 1996).

Importantly, less is known about the *induction* mechanisms underlying different forms of LTP. In particular, how does Ca^{2+} selectively trigger the downstream mechanisms that are appropriate for a particular form of LTP? A preliminary pharmacological study using field recordings suggested that the induction of LTP 1, 2 and 3 required activation of different Ca^{2+} sources: ryanodine receptors (RyRs), inositol 1,4,5-trisphosphate (IP_3) receptors (IP_3Rs), and L-type voltage-dependent Ca^{2+} channels (L-VDCCs), respectively (Raymond & Redman, 2002). While these findings were suggestive, an important question remained unanswered: what characteristic of the Ca^{2+} signals from different sources is responsible for such striking functional specificity? We

 DOI: 10.1113/jphysiol.2005.098947

hypothesized that spatial compartmentalization of Ca^{2+} signals could link different Ca^{2+} sources to the downstream effector mechanisms responsible for the maintenance of each form of LTP. We have tested this hypothesis using whole-cell patch-clamp recordings combined with two-photon Ca^{2+} imaging. For the first time, we have defined the characteristics of Ca^{2+} signals from different sources and in different neuronal compartments during the induction of LTP 1, 2 and 3.

Methods

All experiments were performed in accordance with the Australian National University Animal Experimentation Ethics Committee. Adult male Wistar rats (6–8 weeks) were anaesthetized with halothane, decapitated and the brains were rapidly removed and submerged in ice-cold dissecting solution (mM: 110 choline chloride, 3.2 KCl, 1.25 NaH_2PO_4, 26 $NaHCO_3$, 0.5 $CaCl_2$, 7 $MgCl_2$, 2 ascorbate, 3 pyruvate and 10 D-glucose, equilibrated with 95% O_2/5% CO_2). Transverse hippocampal slices (400 μm) were prepared using a Campden Vibroslice and transferred to a dissecting dish where area CA3 was removed to reduce potential hyperexcitability. Slices were transferred to a holding chamber and submerged in a modified recording solution (mM: 124 NaCl, 3.2 KCl, 1.25 NaH_2PO_4, 26 $NaHCO_3$, 2.5 $CaCl_2$, 1.3 $MgCl_2$, 2 ascorbate, 3 pyruvate and 25 D-glucose, equilibrated with 95% O_2/5% CO_2) maintained at 34°C for 30–40 min, then at room temperature for at least a further 30 min, or until required.

Electrophysiology

Slices for recording were transferred to a submersion brain slice chamber, and perfused in a continuous flow (2 ml min^{-1}) of artificial cerebrospinal fluid (ACSF) (mM: 124 NaCl, 3.2 KCl, 1.25 NaH_2PO_4, 26 $NaHCO_3$, 2.5 $CaCl_2$, 1.3 $MgCl_2$ and 25 D-glucose, equilibrated with 95% O_2/5% CO_2) at 32–33°C. Whole-cell voltage-clamp recordings from CA1 pyramidal cells were made using pulled-glass electrodes (4–5 MΩ) filled with (mM) 135 $KMeSO_4$, 10 Hepes, 10 sodium phosphocreatine, 4 Na-ATP, 0.4 Na-GTP and 4 $MgCl_2$. Resting membrane potentials ranged from −60 to −75 mV, input resistances from 50 to 100 MΩ, and series resistances from 9 to 20 MΩ. Somatic membrane potential was voltage clamped at −65 mV during EPSC recordings. EPSCs were evoked by stimulation of the Schaffer collaterals with 0.1 ms current pulses via a bipolar, Teflon-coated, tungsten electrode. The stimulus amplitude was adjusted while recording in current-clamp mode to produce EPSPs approximately one-third of action potential threshold (5–7 mV), resulting in EPSCs of 200–350 pA.

Experimental recordings were initiated no later than 5 min after whole-cell configuration was obtained. EPSC recordings were made every 15 s for 10 min prior to LTP induction, and for 2 h post-LTP. Series resistance was monitored on-line, and recordings were terminated if this varied more than 20% from the baseline value. LTP was induced by theta-burst stimulation (TBS) consisting of trains of 10 × 100 Hz bursts (5 pulses per burst) with a 200 ms interburst interval, at the test pulse intensity. One train of 10 bursts is denoted as 1 TBS. When multiple trains were delivered (i.e. 4 TBS and 8 TBS) the intertrain interval was 30 s. TBS was delivered while cells were held in current-clamp mode to allow free membrane depolarization from a resting level of approximately −60 mV.

Drugs were either added to the pipette solution (ruthenium red, 40 μM; Sigma, MO, USA), or perfused in the ACSF for 10 min prior to TBS (xestospongin-C, 5 μM (Cayman Chemical Co., MI, USA); nifedipine, 10 μM (Sigma); D-aminophosphonovalerate (D-AP5), 50 μM (Tocris, UK)). Two-tailed Student's *t* tests were used to determine statistical significance at the 95% confidence level. Data are expressed as percentage change from baseline EPSC amplitude (±S.E.M.).

Two-photon Ca^{2+} imaging

Ca^{2+} imaging was performed using a Zeiss LSM 510 imaging system with non-descanned detectors and a 5 W pumped Ti:Sapphire laser ($\lambda = 810$ nm; Coherent). Cells were filled, using whole-cell patch-clamp techniques, with 20 μM Alexa-594 and either 100 μM Oregon Green 488 BAPTA-6F (soma), or 100 μM Oregon Green 488 BAPTA-1 (dendrites/spines; all indicators, Molecular Probes, OR, USA). At least 30 min was allowed for indicator equilibration before imaging commenced. For spine/dendrite recordings, paired-pulse stimulation (PPS; 50 ms interspike interval (ISI), subthreshold for APs) was delivered to the Schaffer collaterals, and small regions of the dendritic tree were successively scanned until an active synapse (producing a visible fluorescence increase in response to PPS) was identified. Line scans (1.5 ms duration, 20 ms intervals) were then obtained through the active spine and a region of underlying dendrite in the same focal plane. For somatic recordings, line scans were obtained through the nuclear region.

PPS-evoked fluorescence changes were recorded in voltage clamp for 400 ms, beginning 50 ms prior to PPS. TBS-evoked fluorescence was then obtained in current clamp for 5 s beginning 500 ms prior to each TBS. Each TBS episode was separated by 30 s. When antagonists were bath applied, PPS recordings were taken prior to, and after 9–10 min of, drug application to provide internal control records. TBS recordings were then made after 10–11 min of drug application. When ruthenium red was applied via the patch pipette, PPS responses were compared with

responses obtained in separate control cells. To replicate the LTP experiments as closely as possible no slice ever received more than eight TBS. Thus, drug-effects on TBS-evoked responses were determined against separate control cells.

Fluorescence (F) across the entire span of the relevant structure(s) was averaged offline. Background fluorescence was not significant, but the photomultiplier tube dark current, measured during a 50 ms period with the laser de-activated, was subtracted. The resting Oregon Green fluorescence measured prior to PPS recordings and prior to each TBS train (F_0) was used as a control for drug-induced changes in resting Ca^{2+} and phototoxicity. Drug-induced changes in resting Ca^{2+} were not observed; however, any record that showed significant increases in resting Ca^{2+} due to phototoxicity was excluded from analysis. For spine and dendrite records, the Alexa-594 fluorescence was used as an additional control for variations in focus or volume of the structures. Data are expressed as percentage $\Delta F/F = [(F - F_0)/F_0]100$. The time integral (area under curve, AUC) of $\Delta F/F$ was used to assess changes in total Ca^{2+}. In some cases the frequency spectrum of the fluorescence signal was obtained from the Fourier transform of $\Delta F/F$.

Results

LTP 1, 2 and 3

Previous studies have shown that repetition of conditioning stimulation can produce LTP of increasing magnitude and persistence (Bliss & Gardner-Medwin, 1973; Huang & Kandel, 1994; Abraham & Huggett, 1997; Raymond & Redman, 2002). Since each of these studies was performed using field recordings, the possibility remained that different populations of neurones maintained different forms of LTP. Therefore, we first sought to characterize the effect of different numbers of conditioning stimuli on LTP in single hippocampal CA1 pyramidal neurones (Fig. 1*A*). We used stimulation protocols that in field recordings are known to induce distinct forms of LTP that depend on different neuronal Ca^{2+} sources (Raymond & Redman, 2002). In these and all subsequent experiments where TBS (see Methods) was delivered, cells were held in current-clamp mode during TBS to allow free membrane depolarization. In control cells, one train of TBS delivered to the Schaffer collaterals induced a weak rapidly decaying LTP that returned to pre-stimulus levels within 2 h post-TBS (Fig. 1*A*; $n = 7$). Increasing stimulation to four trains of TBS resulted in more robust LTP that measured $33 \pm 10\%$ at 2 h post-TBS (Fig. 1*A*; $n = 7$). Finally, 8 TBS induced a similar initial level of potentiation to 4 TBS, but significantly larger LTP at 2 h post-TBS (Fig. 1*A*, $75 \pm 10\%$, $n = 5$). In the absence of TBS, the average percentage change in EPSCs after 130 min of recording was $-10 \pm 7\%$ (Fig. 1*A*; $n = 5$)

Since LTP is generally better classified on the basis of persistence, the post-TBS data for all cells were fit with a double-exponential decay function, as previously described (Raymond *et al.* 2000; Raymond & Redman, 2002). The time constant of decay of the slower exponential (τ) was used as a measure of LTP persistence. The τ values for LTP induced by 1, 4 and 8 TBS were significantly different from one another and mirrored the differences in LTP magnitude (Fig. 1*B*: 1 TBS, 39 ± 8 min ($n = 7$); 4 TBS, 106 ± 13 min ($n = 6$); 8 TBS, 234 ± 38 min ($n = 3$); $P < 0.05$). The 8 TBS τ value is an underestimate since two of five cells showed essentially non-decremental LTP and were consequently excluded from decay analysis. Data from one cell in the 4 TBS group was excluded from decay analysis due to inadequate fit.

The relative differences in magnitude and persistence between the three forms of LTP described here are similar

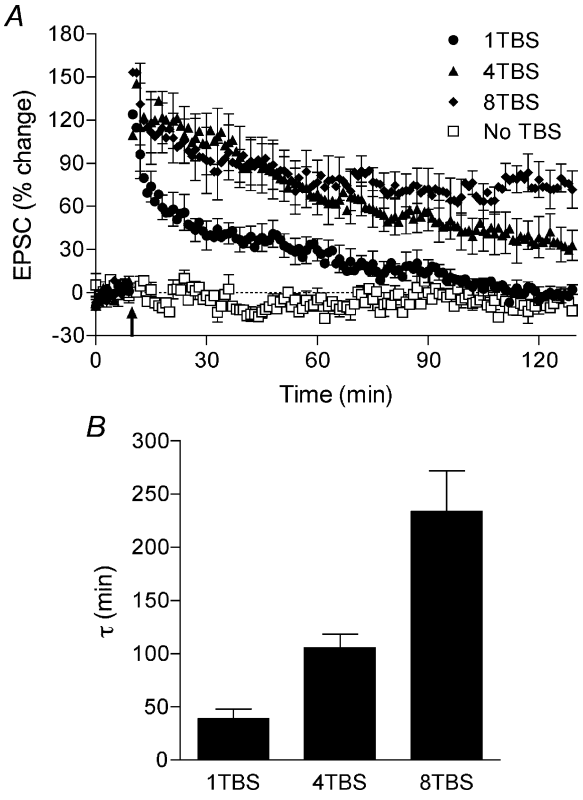

Figure 1. Long-term potentiation (LTP) 1 2, and 3 are induced by increasing numbers of TBS trains
A, summary of whole-cell voltage-clamp recordings showing mean (±S.E.M.) percentage change in EPSC amplitude induced by one, four or eight trains of theta-burst stimulation (1, 4 and 8 TBS) (arrow). Increasing the number of TBS trains resulted in LTP of significantly greater magnitude measured at the 2 h post-TBS time point. *B*, decay characteristics of each form of LTP. The mean time constant of decay (τ, min) is shown for LTP induced by 1, 4 and 8 TBS. Each τ value is significantly different from the others ($P < 0.05$). Increasing numbers of TBS trains induced LTP with slower decay.

to those observed previously using TBS in area CA1 *in vitro* (Abraham & Huggett, 1997; Cohen *et al.* 1998; Raymond & Redman, 2002). Although our data do not allow a categorical definition of these forms of LTP with regard to biochemical maintenance mechanisms, their other characteristics are consistent with the LTP 1, 2 and 3 nomenclature. In the following experiments, pharmacological and Ca^{2+} signalling profiles further justify their classification as distinct forms of LTP, and for convenience we have adopted this nomenclature.

Different Ca^{2+} sources underlie the induction of LTP 1, 2 and 3

Although, under most conditions, NMDA receptor activation appears necessary for the induction of LTP in area CA1, the question of whether it is *sufficient* is less well studied. Previously, we showed that the induction of LTP 1, 2 and 3 in field recordings were dependent on activation of RyRs, IP_3Rs and L-VDCCs, respectively (Raymond & Redman, 2002). In order to directly investigate the Ca^{2+} signalling underlying different forms of LTP, it was necessary to confirm and extend these findings to single CA1 pyramidal neurones.

Inhibition of postsynaptic RyRs with ruthenium red (40 μM) in the recording pipette inhibited LTP induced by 1 TBS such that EPSCs returned to baseline values within 60 min ($-1 \pm 3\%$, $n = 5$; Fig. 2*A* and *B*), and were significantly different from control values at the same time point ($20 \pm 8\%$, $n = 9$, $P < 0.05$). This effect was due to more rapid decay of LTP over the first 60 min post-TBS as indicated by a significant reduction in τ measured over that time period (29 ± 11 min; control, 74 ± 21 min, $P < 0.05$; Fig. 2*B*). In contrast, inhibition of RyRs had no effect on the magnitude or the decay of LTP induced by 4 TBS ($n = 4$) or 8 TBS ($n = 5$; Fig. 2*B*), or on EPSCs in the absence of

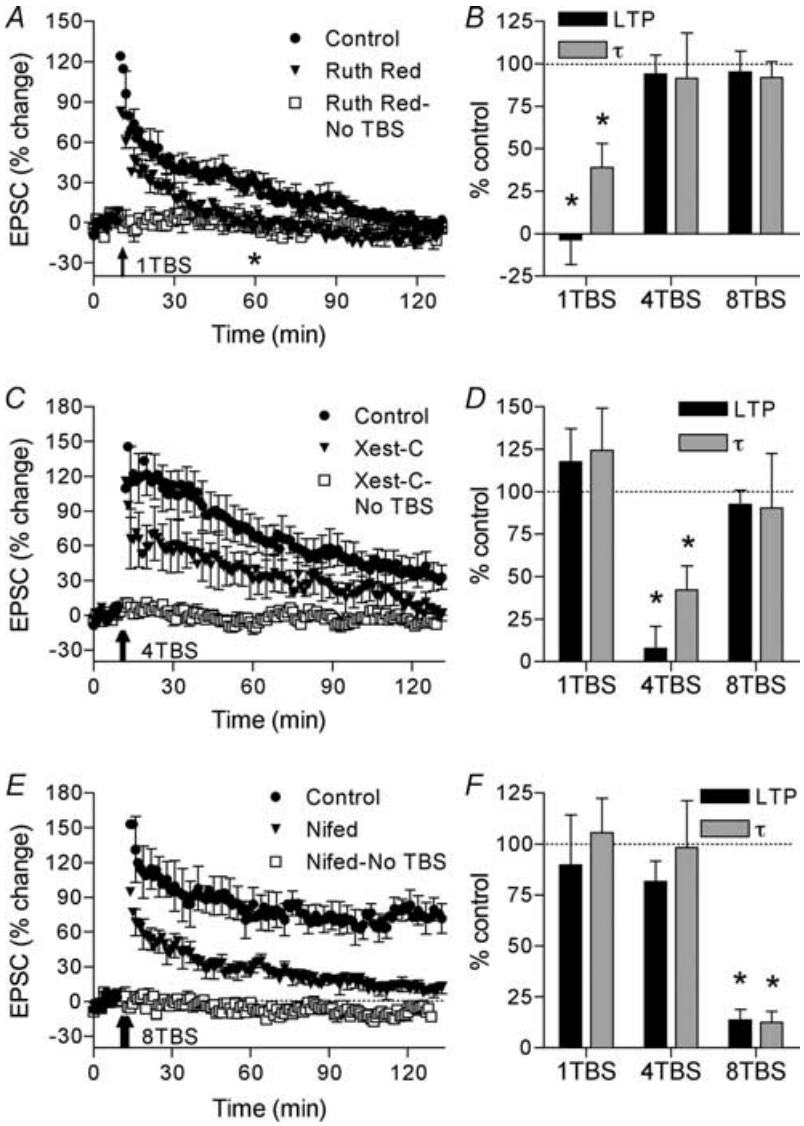

Figure 2. Different Ca^{2+} sources are selectively involved in the induction of LTP 1, 2 and 3
A and *B*, inhibition of ryanodine receptors (RyRs) selectively inhibits LTP 1. *A*, mean (±S.E.M.) percentage change in EPSC amplitude induced by 1 TBS (arrow) in control cells and with ruthenium red (Ruth Red; 40 μM) in the pipette; $^*P < 0.05$. *B*, summary histogram showing mean (±S.E.M.) LTP and τ constants in ruthenium-red-treated cells as percentages of control values for each TBS group. *C* and *D*, inhibition of inositol 1,4,5-trisphosphate (IP_3) receptors selectively inhibits LTP 2. *C*, mean (±S.E.M.) percentage change in EPSCs induced by 4 TBS (arrow) in control cells and cells treated with xestospongin-C (Xest-C; 5 μM, 10 min). *D*, summary histogram as in *B*, but showing the effect of Xest-C on the magnitude and decay of LTP 1, 2 and 3. *E* and *F*, inhibition of L-type voltage-dependent Ca^{2+} channels (VDCCs) selectively inhibits LTP 3. *E*, mean (±S.E.M.) percentage change in EPSCs induced by 8 TBS (arrow) in control cells and cells treated with nifedipine (Nifed; 10 μM, 10 min). *F*, summary histogram as in *B*, but showing the effect of nifedipine on the magnitude and decay of LTP 1, 2 and 3.

TBS ($n = 3$; Fig. 2*A*). Thus, RyRs selectively participate in the induction of LTP 1 in single CA1 pyramidal neurones.

To test the role of IP_3Rs, we bath-applied the selective inhibitor xestospongin-C (Xest-C, 5 μM; Gafni *et al.* 1997). Xest-C had no effect on the magnitude or decay of LTP 1 ($n = 4$) or LTP 3 ($n = 4$; Fig. 2*D*), or on EPSCs in the absence of TBS ($n = 3$; Fig. 2*C*). However, blockade of IP_3Rs selectively inhibited LTP 2, with EPSCs returning to baseline within 2 h ($3 \pm 4\%$, $n = 4$, $P < 0.05$; Fig. 2*C*) and τ decreasing from 106 to 45 min ($P < 0.05$; Fig. 2*D*). Thus, IP_3Rs are selectively involved in the induction of LTP 2 in single CA1 pyramidal neurones.

L-VDCCs have been shown to be important for the induction of LTP under conditions of intense conditioning stimulation (Grover & Teyler, 1990; Impey *et al.* 1996; Morgan & Teyler, 2001; Raymond & Redman, 2002). In single CA1 pyramidal neurones, inhibition of L-VDCCs with nifedipine (10 μM) had no effect on the magnitude or persistence of either LTP 1 ($n = 4$) or LTP 2 ($n = 4$; Fig. 2*F*), or on EPSCs in the absence of TBS ($n = 3$; Fig. 2*E*). In contrast, L-VDCC blockade inhibited LTP 3 (Fig. 2*E* and *F*). At 2 h post-TBS, EPSCs were only $10 \pm 4\%$ larger than baseline and τ was reduced to just 29 min ($n = 6$, $P < 0.05$). These findings reveal a selective requirement for L-VDCCs in the induction of LTP 3.

Hypotheses

The data described above show that different Ca^{2+} sources are remarkably selective for the induction of different forms of LTP, even within a single neurone. Each Ca^{2+} source appears to be narrowly tuned to the induction of a specific form of LTP with defined magnitude and decay characteristics. We developed two alternative hypotheses to explain these findings. In the 'Threshold' hypothesis, the induction each form of LTP requires a specific threshold Ca^{2+} signal. As the number of TBS trains is increased, different Ca^{2+} sources are successively recruited to surpass these thresholds. In this case, the form of LTP induced is determined by some characteristic of the overall Ca^{2+} signal, e.g. peak amplitude or time integral. The 'Compartmental' hypothesis proposes a spatial mechanism for linking Ca^{2+} to LTP. That is, the specific location of Ca^{2+} signals within the neurone is the major determinant of the form of LTP induced. In this case, the effector mechanisms underlying each form of LTP are colocalized with, and preferentially activated by, a particular Ca^{2+} source. To test these hypotheses we performed two-photon Ca^{2+} imaging during TBS, and recorded Ca^{2+} signals from three different neuronal compartments in the presence and absence of various Ca^{2+} source antagonists.

Spine Ca^{2+} correlates with LTP 1

Spine Ca^{2+} dynamics have commonly been implicated in the induction of synaptic plasticity (Bliss & Collingridge, 1993; Lynch, 2004). We hypothesized that spine Ca^{2+} is particularly important for the induction of LTP 1 since the key kinases involved in LTP 1 maintenance (e.g. CaMKII and protein kinase C) are highly expressed in the post-synaptic density (Kennedy, 2000). Furthermore, in CA1 pyramidal neurones, spines appear particularly enriched with RyRs (Sharp *et al.* 1993), which our results show to be important for the induction of LTP 1 (see above and Raymond & Redman, 2002).

Changes in spine Ca^{2+} during TBS were measured using line scans through synaptically active spines and their parent dendrites (Fig. 3*A*). To locate synaptically active spines, the neurone was voltage clamped at -65 mV and PPS (50 ms ISI, subthreshold for APs) was delivered to the Schaffer collaterals. PPS was used so as to avoid preconditioning effects of stronger stimulation protocols, necessitating the use of a high-affinity Ca^{2+} indicator in these experiments. Small regions of the dendritic tree were imaged until a spine showing a stimulus-locked fluorescence increase was observed (Fig. 4). Cells were then held in current-clamp mode during TBS. In controls, TBS resulted in a fast rise in Ca^{2+} followed by periodic peaks corresponding with bursts of synaptic activity (Fig. 3*A* and *B*). There were no significant differences in the total area of spine Ca^{2+} responses produced by each of 8 TBS trains (area under curve (AUC) first TBS: 328 ± 58, $n = 7$; fourth TBS: 334 ± 75, $n = 7$; eighth TBS: 260 ± 119, $n = 4$). In addition, resting Ca^{2+}, measured by the resting *green* fluorescence as a percentage of the corresponding Alexa-594 *red* fluorescence (G/R $\times$ 100%), did not vary significantly from the first to the eighth TBS (first TBS: $34 \pm 7\%$, $n = 7$; eighth TBS: $37 \pm 6\%$, $n = 4$).

Analysis of the total area of individual spine Ca^{2+} transients evoked by each TBS train revealed no significant effect of any of the pharmacological agents (Student's *t* tests, $P > 0.05$). However, we noted that the spine Ca^{2+} signal included two components: periodic peaks overlaid on a more constant signal. Qualitatively, ruthenium red appeared to selectively inhibit the peaks, while leaving the underlying component intact (Fig. 3*B*). To investigate this possibility we performed Fourier analyses on spine Ca^{2+} transients as a method of separating the two components. In control cells, a large peak in energy at 5 Hz confirmed that spine Ca^{2+} was indeed modulated at the burst frequency of TBS (Fig. 3*C*, data from first TBS), and this effect was constant across all 8 TBS trains (average magnitude at 5 Hz $= 1265 \pm 350$; Fig. 3*F*, black bars). Inhibition of RyRs significantly reduced the magnitude of the 5 Hz peak across all 8 TBS trains (average magnitude at 5 Hz $= 415 \pm 84$, first to fifth TBS $n = 7$, sixth to eighth TBS $n = 5$, individual comparisons all $P < 0.05$;

Fig. 3*C* and *F*). In contrast, inhibition of IP_3Rs (average magnitude = 910 ± 245, first to fourth TBS $n = 6$, fifth to eighth TBS $n = 4$; Fig. 3*D* and *G*) or L-VDCCs (average magnitude = 942 ± 295, $n = 4$ for each TBS; Fig. 3*E* and *H*) had no significant effect on individual 5 Hz peak comparisons.

Since ruthenium red is only effective in blocking LTP 1, its effect on the first TBS-evoked Ca^{2+} transient is relevant with regard to LTP induction. For LTP 2 and 3, induced by multiple trains, it is possible that some cumulative effect of Ca^{2+} across trains is involved in their induction; in which case, non-significant drug effects on individual

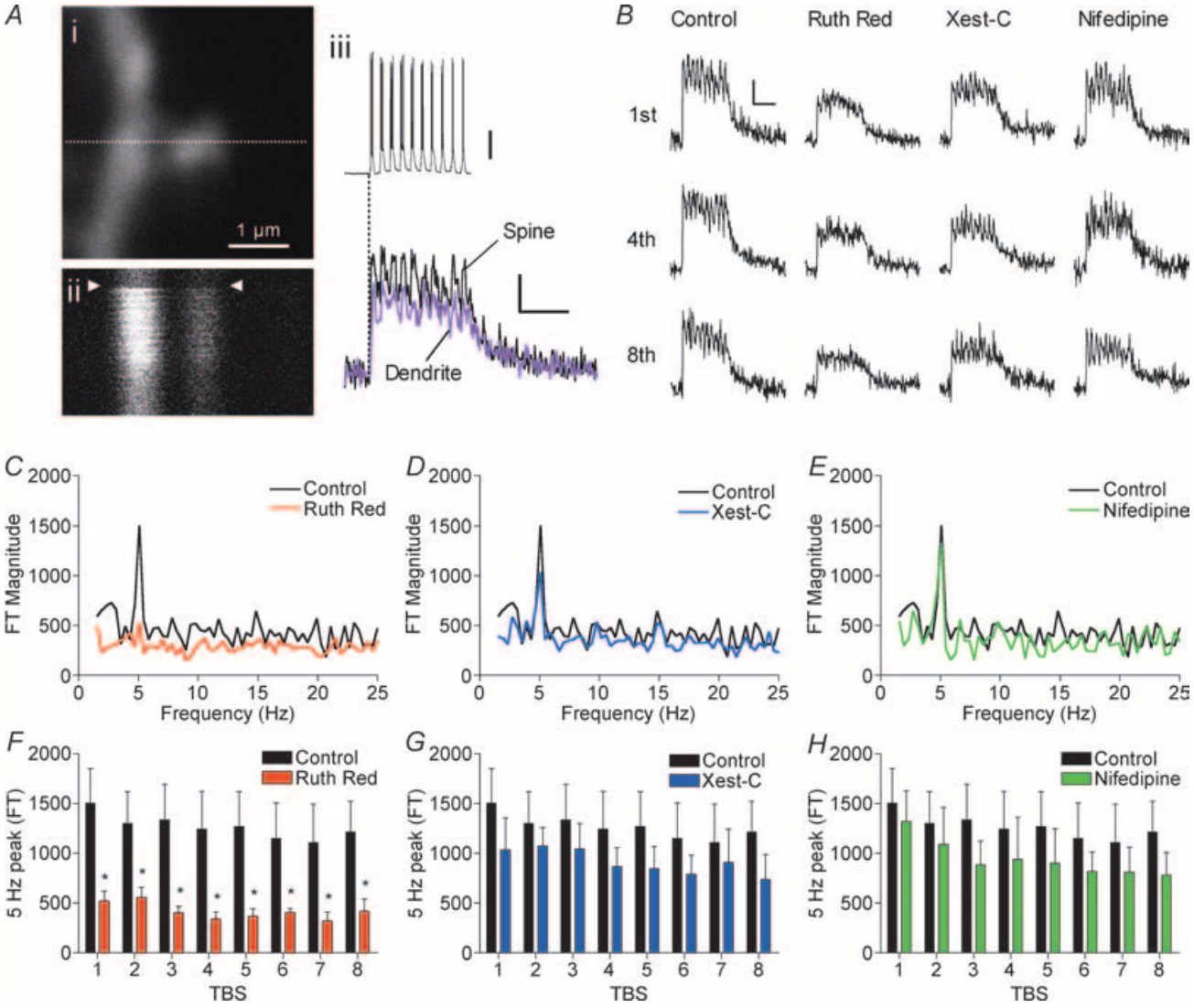

Figure 3. Inhibition of RyRs selectively inhibits a component of spine Ca^{2+} signals
A, section of the apical dendrite of a CA1 pyramidal neurone filled with Oregon Green 488 BAPTA 1 and Alexa-594 showing positioning of line scan through a spine and the underlying dendrite (i); ii, line scan time-series during 1 TBS beginning at arrowheads; iii, current-clamp record during 1 TBS (upper trace; scale bar, 20 mV) aligned with mean $\Delta F/F$ (where F is fluorescence) measured simultaneously in the spine (black) and dendrite (purple; scale bars, 50% and 1 s). *B*, mean $\Delta F/F$ traces showing change in $[Ca^{2+}]$ in the spine during the first, fourth and eighth TBS trains in controls and drug-treated cells (scale bars, 50%, 1 s). Notice the loss of the Ca^{2+} peaks in the presence of ruthenium red. *C–E*, examples of Fourier transform (FT) analyses on spine Ca^{2+} transients produced by 1 TBS in controls and drug-treated cells. Notice that the prominent peak at 5 Hz, which corresponds to the burst frequency of TBS, is eliminated by ruthenium red (*C*), but not by xestospongin-C (*D*) or nifedpine (*E*). *F–H*, summary histograms of the mean (±S.E.M.) magnitude of the 5 Hz peak obtained by Fourier analysis in controls and cells treated with ruthenium red (*F*), xestospongin-C (*G*), and nifedipine (*H*); $^*P < 0.05$. Ruthenium red selectively blocks the 5 Hz peak in the spine Ca^{2+} transients produced by each of 8 TBS trains.

spine Ca^{2+} transients may be biologically significant when compounded across 4 TBS or 8 TBS. To test this we performed two-way ANOVA on the area of Ca^{2+} transients across the relevant number of trains for each antagonist: four trains for Xest-C since it selectively inhibits LTP induced by 4 TBS, and eight trains for nifedipine since it inhibits LTP induced by 8 TBS. In agreement with the individual comparisons, there was no significant effect of Xest-C on spine Ca^{2+} across 4 TBS ($P > 0.05$, $F_{1,42} = 3.57$). However, ANOVA did reveal a significant effect of nifedipine when analysed across all 8 TBS trains ($P < 0.05$, $F_{1,68} = 6.17$).

None of the pharmacological agents had a significant effect on resting Ca^{2+} (G/R). For Xest-C and nifedipine, G/R measurements were made prior to (Xest-C, 41 ± 5%, $n = 6$; nifedipine, 32 ± 6%, $n = 7$) and after 10 min of drug application (Xest-C, 39 ± 5%, $n = 6$; nifedipine, 32 ± 6%, $n = 7$). With ruthenium red in the recording pipette, comparison of G/R was made against a separate control group (ruthenium red, 38 ± 8%, $n = 6$; control, 34 ± 7%, $n = 7$).

These data show that during TBS, RyRs release pulses of Ca^{2+} in the spine, phase-locked to the pattern of synaptic activity. Under these conditions, IP_3Rs and L-VDCCs do not observably contribute to individual TBS-evoked spine Ca^{2+} signals. L-VDCCs do, however, appear to underlie a weak spine Ca^{2+} signal that is only apparent when analysed cumulatively across 8 TBS trains. This pharmacological profile is consistent with a role for spine Ca^{2+} in the induction of LTP 1, but not LTP 2. Although nifedipine does not affect individual TBS-evoked transients, we cannot rule out the involvement of a weak cumulative spine signal in the induction of LTP 3. It is important to note that even when RyRs are blocked, there is a considerable residual Ca^{2+} signal in the spine (Fig. 3*B*). This underlying signal is possibly mediated by NMDA receptors (NMDARs) or non-L-type VDCCs activated by back-propagating APs (Sabatini & Svoboda, 2000; Yasuda *et al.* 2003).

An interesting side issue is the role of different Ca^{2+} sources in spine transients produced by weak stimulation. PPS, subthreshold for AP generation, produced observable Ca^{2+} transients in some spines (Fig. 4*A*). Inhibition of RyRs ($n = 8$), IP_3Rs ($n = 6$) or L-VDCCs ($n = 7$) had no significant effect on spine Ca^{2+} transients produced by PPS. On the other hand, inhibition of NMDARs completely abolished these transients ($n = 4$; Fig. 4*B*). These findings are in contrast to observations in organotypic cultures (Emptage *et al.* 1999), but agree with other studies of spine Ca^{2+} evoked by single EPSPs (reviewed by Sabatini *et al.* 2001). Together, our data show that LTP-inducing TBS recruits additional mechanisms for Ca^{2+} signalling in the spine compared with single or paired subthreshold stimuli.

Dendritic Ca^{2+} correlates with LTP 2

The second neuronal compartment we investigated was the region of dendrite from which the synaptically active spine arose. LTP 2 is dependent on protein translation from pre-existing mRNA (Otani *et al.* 1989; Raymond *et al.* 2000), the machinery for which has been shown to be located in dendrites beneath postsynaptic sites (Steward & Schuman, 2001). Moreover, IP_3Rs, upon which LTP 2 induction depends, appear to be preferentially located in dendritic shafts in CA1 pyramidal neurones (Sharp *et al.* 1993).

Dendritic Ca^{2+} measurements were obtained simultaneously with the spine recordings (see Fig. 3*A*). Control responses in dendrites were similar in shape to spine responses although $\Delta F/F$ was slightly smaller (average AUC across all 8 TBS 262 ± 78, $n = 6$; Figs 3*A* and 5*A*). Resting Ca^{2+} assessed by G/R measurements in dendritic compartments did not vary significantly from the first TBS (29 ± 9%, $n = 7$) to the eighth TBS (32 ± 9%, $n = 6$). To separate different components of the dendritic signals we again performed Fourier analyses, which revealed a peak at 5 Hz, similar to, albeit smaller than, the spine waveforms. However, unlike in the spine, none of the Ca^{2+} source antagonists had any significant effect on the dendritic 5 Hz peak (Fig. 5*B–D*). Inhibition of RyRs ($n = 6$; Fig. 5*E*) or L-VDCCs ($n = 4$; Fig. 5*G*) also had no significant effect on the area of individual dendritic

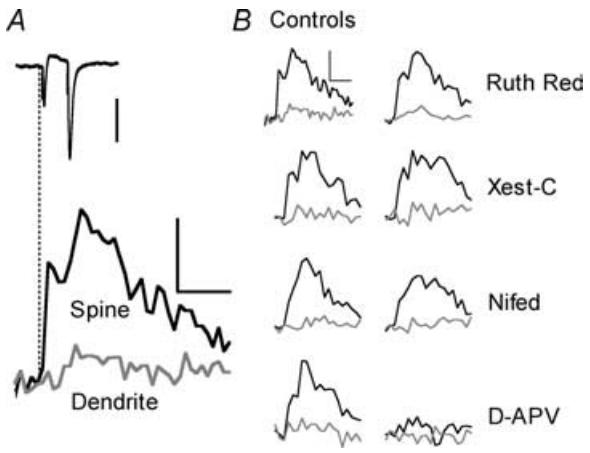

Figure 4. Spine and dendrite Ca^{2+} transients evoked by paired-pulse stimulation
A, voltage-clamp record during paired-pulse stimulation (upper trace; scale bar, 250 pA) aligned with mean $\Delta F/F$ measured simultaneously in spines (black) and dendrites (grey; scale bars, 50% and 100 ms). *B*, mean $\Delta F/F$ traces showing the effect of different Ca^{2+} antagonists on paired-pulse evoked Ca^{2+} transients in spines (black) and dendrites (grey; scale bars, 50% and 100 ms). Within-group controls for each antagonist are shown on the left, except for ruthenium red, which is compared with a separate control group. Only D-aminophosphonovalerate (D-AP5; 50 μM) caused any significant change in Ca^{2+} transients evoked by subthreshold paired-pulse stimulation.

Ca^{2+} responses to any of the 8 TBS trains (Student's *t* tests, $P > 0.05$). In addition, two-way ANOVA revealed no significant cumulative effect of nifedipine across 8 TBS ($P > 0.05$, $F_{1,59} = 3.51$). However, inhibition of IP_3Rs significantly reduced the area of individual Ca^{2+} transients from the second TBS through to the eighth (average AUC 84 ± 33, second to fourth TBS $n = 6$, fifth to eighth TBS $n = 5$, individual comparisons all $P < 0.05$), with no significant effect on the first TBS response (166 ± 25, $n = 6$; Fig. 5*A* and *F*).

As observed in the spine measurements, none of the pharmacological agents affected resting Ca^{2+} (ruthenium red, 35 ± 10%, $n = 6$; control, 31 ± 9%, $n = 6$; pre-Xest-C, 35 ± 2%, $n = 5$; post-Xest-C, 34 ± 2%, $n = 5$;

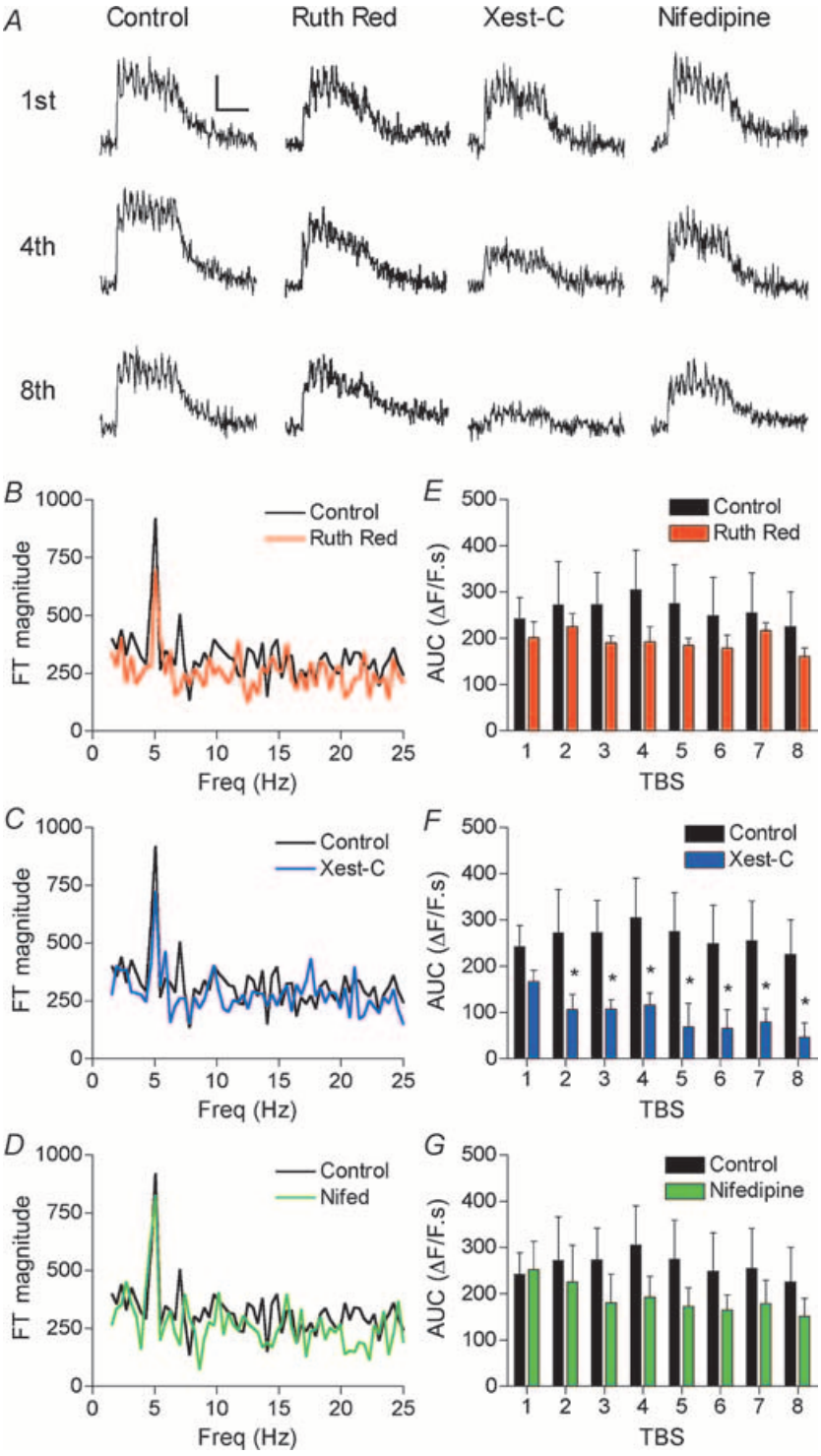

Figure 5. Inhibition of IP_3 receptors selectively inhibits dendritic Ca^{2+} signals
A, mean dendritic Δ*F*/*F* traces showing change in [Ca^{2+}] in the dendrite during the first, fourth and eighth TBS trains, in controls and drug-treated cells (scale bars, 50% and 1 s). Notice the selective inhibition by xestospongin-C during the fourth and eighth trains. *B–D*, examples of Fourier transform (FT) analyses on dendritic Ca^{2+} transients produced by 1 TBS in controls and cells treated with ruthenium red (*B*), xestospongin-C (*C*) and nifedipine (*D*). The 5 Hz peak in dendritic Ca^{2+} transients is unaffected by any of the antagonists. *E–G*, summary histograms of the mean (±S.E.M.) area under the curve (AUC; time integral) of dendritic Ca^{2+} transients in controls and cells treated with ruthenium red (*E*), xestospongin-C (*F*) and nifedipine (*G*); $^*P < 0.05$. Xestospongin-C selectively inhibits the dendritic Ca^{2+} transients produced by the second to the eighth TBS.

pre-nifedipine, 28 ± 5%, $n = 4$; post-nifedipine, 29 ± 5%, $n = 4$).

These findings show that IP_3R-mediated Ca^{2+} release is responsible for a significant component of TBS-evoked dendritic Ca^{2+} signals. RyRs and L-VDCCs do not observably contribute to dendritic Ca^{2+} over the course of stimulus protocols that are relevant to their role in LTP. This pharmacological profile is consistent with a role for dendritic Ca^{2+} in the induction of LTP 2, but not LTP 1 or LTP 3. Again, it is important to note that there is a significant residual Ca^{2+} signal when IP_3Rs are inhibited, and that this signal is likely to be due to activation of non-L-type VDCCs and/or NMDARs.

Somatic Ca^{2+} correlates with LTP3

Since the maintenance of LTP 3 is dependent on gene transcription (Nguyen *et al.* 1994; Frey *et al.* 1996) we recorded somatic Ca^{2+} transients using line scans through the nuclear region (Fig. 6*A*). In control cells the first train of TBS produced a moderate increase in Ca^{2+} that continued to rise throughout the stimulus train (AUC 42 ± 13, $n = 8$; Fig. 6*B*). Ca^{2+} responses to subsequent TBS trains were significantly elevated over the 1 TBS signal and remained similar in magnitude and area across trains 2–8 (fourth TBS, AUC 79 ± 15, $n = 8$, $P < 0.05$; eighth TBS, AUC 72 ± 11, $n = 8$, $P < 0.05$; Fig. 6*B* and *C*). Resting G/R did not vary significantly from the first TBS (18.2 ± 0.3%, $n = 8$) to the eighth TBS (18.0 ± 0.4%, $n = 8$).

Inhibition of RyRs ($n = 5$; Fig. 6*B* and *C*) or IP_3Rs ($n = 4$; Fig. 6*B* and *D*) had no effect on the area of somatic Ca^{2+} transients produced by any of the 8 TBS trains. Furthermore, Xest-C had no significant cumulative effect on somatic Ca^{2+} over 4 TBS ($F_{1,40} = 0.05$, $P > 0.05$). However, blocking L-VDCCs with nifedipine (10 μM) resulted in substantial reductions in somatic Ca^{2+} (Fig. 6*B* and *E*). The greatest effect was on the first Ca^{2+} transient which showed a 75 ± 8% reduction in area, and 50–60%

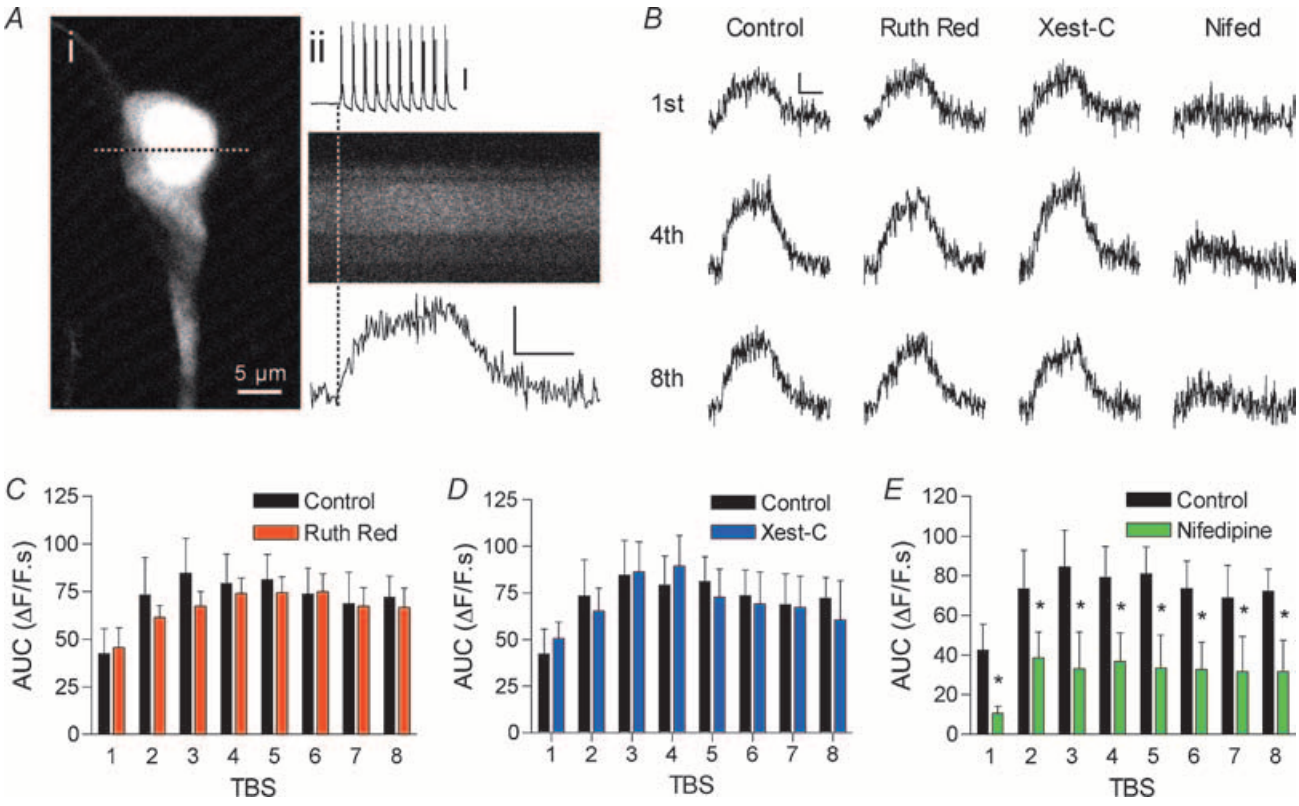

Figure 6. Inhibition of L-type VDCCs selectively inhibits somatic Ca^{2+} signals
A, CA1 pyramidal neurone filled with Oregon Green 488 BAPTA 6-F and Alexa-594 showing positioning of line scan through the nucleus (i); ii, current-clamp record during 1 TBS (upper trace; scale bar, 20 mV), aligned with line scan time-series (middle trace) and $\Delta F/F$ averaged over the entire nucleus (lower trace; scale bars, 20% and 1 s). *B*, mean somatic $\Delta F/F$ traces showing change in $[Ca^{2+}]$ during the first, fourth and eighth TBS trains in controls and drug-treated cells (scale bars, 10% and 1 s). *C–E*, summary histograms of the mean (±S.E.M.) time integral (AUC) of somatic Ca^{2+} transients produced by each TBS train in controls and cells treated with ruthenium red (*C*), xestospongin-C (*D*) and nifedipine (*E*); $^*P < 0.05$. Note that somatic Ca^{2+} transients are selectively inhibited by nifedipine.

inhibition was observed across the subsequent trains ($n = 4$ each, $P < 0.05$). The pharmacological profile of somatic Ca^{2+} transients is consistent with a role in the induction of LTP 3, but not LTP 1 or 2. Taken together, the imaging data provide strong support for the 'Compartmental' hypothesis of LTP induction, suggesting that different Ca^{2+} sources generate localized signals that selectively activate effector mechanisms underlying specific forms of LTP.

The NMDA receptor gates LTP 1 and LTP 2 by regulating Ca^{2+} release from internal stores

The data so far show that antagonists of RyRs, IP_3Rs and L-VDCCs inhibit Ca^{2+} signals in specific spatial locations to selectively prevent the induction of different forms of LTP. Thus, questions arise regarding the role of the NMDA receptor in the induction of each form of LTP, and in the generation of the underlying Ca^{2+} signals. Inhibition of NMDA receptors with D-AP5 (50 μM) reduced the early post-tetanic potentiation (PTP) produced by 1 TBS and completely inhibited LTP beyond ~50 min post-TBS ($-3 \pm 5\%$ 60 min post-TBS, $n = 4$, $P < 0.05$; Fig. 7*A*). A similar effect was observed on LTP 2, with weak PTP and no potentiation beyond 60 min post-TBS ($-2 \pm 2\%$, $n = 5$, $P < 0.05$; Fig. 7*B*). LTP 3 was less sensitive to NMDAR blockade (Fig. 7*C*). The PTP produced by 8 TBS was reduced to a similar degree as that observed for LTP 1 and LTP 2, but a slow potentiation of EPSCs developed over 20–30 min post-TBS, before settling to a level ($35 \pm 3\%$, $n = 5$, Fig. 7*C*) that was less than control ($75 \pm 10\%$, $n = 5$, $P < 0.05$), but greater than nifedipine-treated cells at 2 h post-TBS ($10 \pm 4\%$, $n = 6$, $P < 0.05$). These data demonstrate that NMDAR activation is necessary for LTP 1 and LTP 2, but that LTP 3 incorporates a significant NMDAR-independent component.

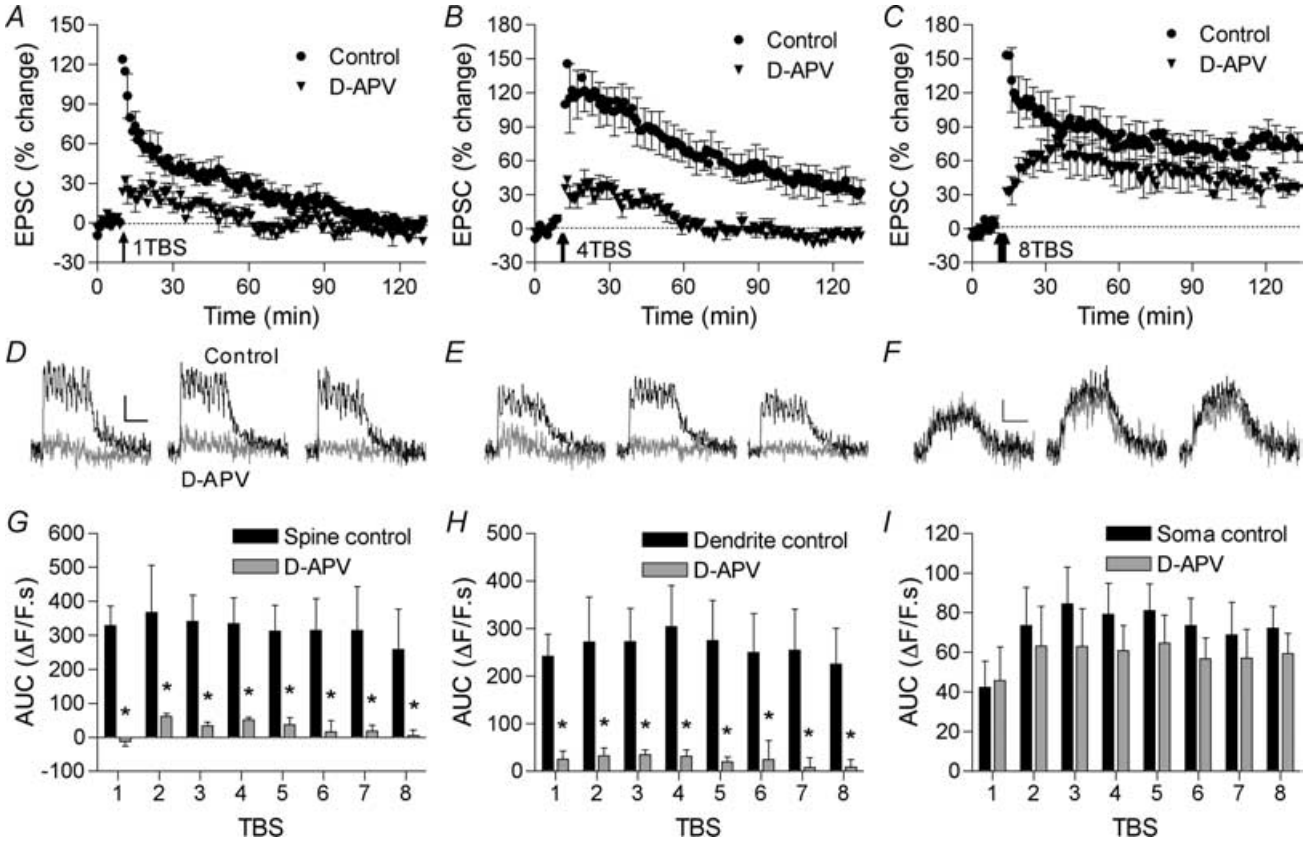

Figure 7. Inhibition of NMDA receptors blocks LTP 1 and 2, and inhibits spine and dendritic Ca^{2+} signals
A–C, summary of whole-cell voltage-clamp recordings showing the effect of D-AP5 (50 μM, 10 min) on LTP 1 (*A*), LTP 2 (*B*) and LTP 3 (*C*) over a 2 h post-TBS period. TBS was delivered at the times indicated by the arrows. Inhibition of NMDA receptors inhibits LTP 1 and LTP 2, but only partially affects LTP 3. *D–F*, mean $\Delta F/F$ traces showing the effect of D-AP5 (50 μM) on Ca^{2+} transients produced by the first, fourth and eighth TBS trains in spines (*D*), dendrites (*E*) and soma (*F*). Scale bars, 50% and 1 s (*D* and *E*), and 10% and 1 s (*F*). *G–I*, summary histograms showing the effect of D-AP5 on the mean (±S.E.M.) time integral (AUC) of Ca^{2+} transients in spines (*G*), dendrites (*H*) and soma (*I*); $^*P < 0.05$. Inhibition of NMDA receptors completely abolishes spine and dendrite Ca^{2+} signals, but has no effect on somatic Ca^{2+}.

Given that both NMDA and non-NMDA Ca^{2+} sources appear necessary for the induction of LTP, an important question is how, or even whether, they interact to generate the underlying Ca^{2+} signal. Inhibition of NMDA receptors with D-AP5 (50 μM) virtually abolished TBS-induced Ca^{2+} transients in spines ($n = 4$, $P < 0.05$; Fig. 7*D* and *G*) and dendrites ($n = 4$, $P < 0.05$; Fig. 7*E* and *H*), consistent with inhibition of LTP 1 and LTP 2. Combined with our demonstration of the role for Ca^{2+} stores in these compartments, these data suggest that in response to TBS, NMDAR activation triggers Ca^{2+} release from internal stores. At the soma, D-AP5 had no significant effect on individual TBS-induced Ca^{2+} transients ($n = 4$; Fig. 7*F* and *I*) and ANOVA revealed no significant cumulative effect across all 8 TBS ($F_{1,79} = 1.95$, $P > 0.05$), suggesting that the small effect of D-AP5 on LTP-3 is due either to a reduction in Ca^{2+} that is below our detection levels, or to inhibition of Ca^{2+} elsewhere in the neurone.

Discussion

We have shown that different forms of LTP that are dependent on different Ca^{2+} sources coexist at CA3–CA1 synapses and, more importantly, that the Ca^{2+} signals emanating from these discrete sources are spatially segregated. During LTP-inducing stimulation, RyRs contribute selectively to spine Ca^{2+} and are required for LTP 1, IP_3Rs produce Ca^{2+} signals in the dendrites and are required for LTP 2, and L-VDCCs generate somatic Ca^{2+} responses and are required for LTP 3. LTP 3 may additionally involve a weak spine signal that only becomes apparent when compounded over 8 TBS trains. We interpret these findings as support for the 'Compartmental' hypothesis in which Ca^{2+} signals in discrete locations selectively induce different forms of LTP. This represents an elegant mechanism for the selective activation of multiple independent cellular processes by a single second-messenger.

Immunohistochemical studies in CA1 pyramidal neurones largely support the spatial segregation revealed by Ca^{2+} imaging. RyRs appear to be located primarily in spines and dendritic shafts close to spines, whereas IP_3Rs seem absent from spines but are highly expressed in dendritic shafts (Sharp *et al.* 1993). L-VDCCs are predominantly found on cell bodies and proximal dendrites (Westenbroek *et al.* 1990; Hell *et al.* 1996), although they have recently been described on proximal dendritic spines (Davare *et al.* 2001). Electrophysiological analyses suggest that L-VDCCs have a more proximal distribution, whereas distal dendrites contain mainly T- and R-type VDCCs (Christie *et al.* 1995; Magee & Johnston, 1995). Imaging experiments show that spines do display VDCC-mediated Ca^{2+} transients, but these appear to be via the R-type (Sabatini & Svoboda, 2000; Yasuda *et al.* 2003).

It should be noted that such strict segregation of Ca^{2+} channels is not a requirement for the spatial encoding model presented here. Indeed, each of the Ca^{2+} antagonists produces an inhibitory trend in Ca^{2+} transients in all three compartments. This could indicate that each Ca^{2+} source is ubiquitously expressed, but with a relative preponderance of one channel type over others within a particular compartment.

Spine Ca^{2+} and LTP 1

Our data suggest that activation of postsynaptic NMDARs during TBS triggers Ca^{2+}-induced Ca^{2+} release (CICR) via RyRs located in the spine, thereby acting as a gate for the induction of LTP 1 (Fig. 8). Previous studies have shown that spine Ca^{2+} evoked by weak, subthreshold synaptic stimulation is predominantly generated via NMDARs (but see Emptage *et al.* 1999; reviewed by Sabatini *et al.* 2001). We confirm this by showing that spine Ca^{2+} transients evoked by subthreshold paired-pulse stimulation are not sensitive to antagonists of internal Ca^{2+} release, or L-VDCCs, but are completely blocked by D-AP5. In contrast, the much stronger TBS recruits a significant RyR-mediated component that is gated by NMDARs. While one previous study has shown that AP5 blocks tetanus-induced spine Ca^{2+} transients (Petrozzino *et al.* 1995), this is the first time that the contribution of RyRs to tetanus-induced spine Ca^{2+} has been revealed.

CICR produces peaks of Ca^{2+} in the spine that are associated with bursts of neuronal activity generated by TBS. The significant underlying, RyR-*insensitive* component is largely blocked by D-AP5, which could reflect Ca^{2+} entry directly through NMDARs. Alternatively, NMDAR-mediated depolarization could regulate R-type VDCC activity that may contribute to the overall spine signal (Sabatini & Svoboda, 2000; Yasuda *et al.* 2003). It is unclear what role back-propagating bAPs are playing in TBS-evoked spine Ca^{2+} signals. The weak L-VDCC-mediated spine signal revealed by ANOVA across 8 TBS may well be activated by bAPs, but is clearly not important for the induction of LTP 1. Our data suggest that in response to TBS, Ca^{2+} generated directly by bAPs is of lower magnitude relative to contributions from other sources activated by TBS. However, further study is required to investigate this possibility more thoroughly.

At this point, it is prudent to note that the use of weak PPS to locate synaptically active spines without preconditioning the synapses required the use of a high-affinity Ca^{2+} indicator in the spine and dendrite recordings. Under these conditions, it is possible that the Ca^{2+} transients are underestimated due to indicator saturation. If this is the case, weak contributions of L-VDCCs or IP_3Rs to the 5 Hz peaks may not have been detected. On the other hand, the contribution of RyRs

could well be even more robust than described here. Thus, these experiments reveal the dominant TBS-evoked Ca^{2+} signalling pathways in spines and dendrites.

Due to the limited resolution of light microscopy, we have selected rather large neuronal compartments for our analysis. However, it is likely that the signalling domains involved are much smaller, enabling very precise links to effector systems. NMDARs are clustered at the Postsynoptic density (PSD) by an interaction with the Postsynoptic density (PSD) protein Shank and the linking protein Homer (Tu *et al.* 1999; Sala *et al.* 2001). Recently, it has been shown that Homer can also bind RyRs (Feng *et al.* 2002), suggesting that NMDARs and RyRs may be colocalized in a Ca^{2+} microdomain, maintained by interactions between several PSD and scaffolding proteins. The burst-like release of Ca^{2+} via RyRs in this microdomain could be well suited to activating CaMKII, which is situated in the PSD (Kennedy, 2000), is preferentially activated by pulses of Ca^{2+} (De Koninck & Schulman, 1998), and is a key enzyme in the post-translational modifications that underlie LTP 1 (Bliss & Collingridge, 1993).

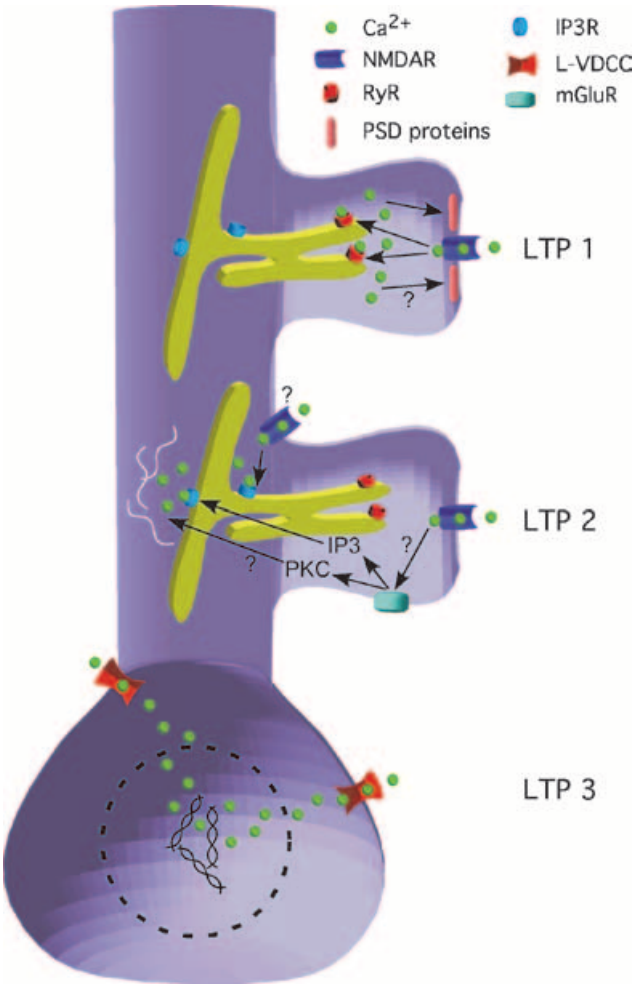

Figure 8. Spatial encoding model for the induction of LTP 1, 2 and 3
Schematic diagram describing a proposed mechanism for the differential induction of different forms of LTP by Ca^{2+}. Weak conditioning stimulation (e.g. 1 TBS) activates NMDARs resulting in a modest influx of Ca^{2+} into the spine, which in turn activates Ca^{2+}-induced Ca^{2+} release (CICR) via ryanodine receptors (RyR). CICR is proposed to activate kinases in the PSD that underlie the expression of LTP 1. Stronger stimulation (e.g. 2–4 TBS) can additionally recruit an IP_3-dependent signalling pathway by activation of mGluRs. Ca^{2+} release from IP_3Rs in the dendrites, possibly combined with other G-protein-coupled mechanisms (e.g. protein kinase C (PKC)), is proposed to activate local dendritic protein synthesis that supports the expression of LTP 2. The NMDAR gates IP_3R activation, possibly via extrasynaptic NMDARs. Repetitive activation of L-VDCCs (e.g. by 5–8 TBS) causes significant Ca^{2+} peaks in the nucleus, which are proposed to trigger the gene transcription necessary for the expression of LTP 3.

Dendritic Ca^{2+} and LTP 2

Our data suggest that LTP 2 is induced by release of Ca^{2+} via IP_3Rs located in the dendrites (Fig. 8). LTP 2 and IP_3R-mediated dendritic Ca^{2+} release are also completely dependent on NMDAR activation. Thus, similar to the situation for LTP 1, NMDARs appear to gate the induction of LTP 2 via a permissive action on IP_3R-mediated Ca^{2+} release.

How might NMDARs gate IP_3R-mediated Ca^{2+} release? Previous work has shown that LTP 2 induction is dependent on activation of group 1 mGluRs (Raymond *et al.* 2000). In a series of studies Nakamura and colleagues have characterized an mGluR/IP_3R-dependent dendritic Ca^{2+} signal that is synergistically activated by Ca^{2+} influx during depolarization (Nakamura *et al.* 1999, 2000, 2002). In distal oblique dendrites, where the majority of the present recordings were made, Nakamura *et al.* (2002) showed that NMDARs are involved in coactivating IP_3Rs, even in the absence of VDCC activity. Our data are consistent with this model in that dendritic Ca^{2+} signals were almost completely blocked by D-AP5. In this case, it is not clear whether Ca^{2+} entering via the NMDAR acts directly on IP_3Rs, or on some part of the IP_3 production cascade. Since synaptic NMDARs are a considerable distance from the parent dendrite, it is possible that extrasynaptic NMDARs (Lozovaya *et al.* 2004) are important in this regard (Fig. 8). In the present study there appears to be minimal diffusion of Ca^{2+} from the spine to the dendrite, since RyRs, which are colocalized with NMDARs in spines, did not affect dendritic Ca^{2+} signals. Nakamura *et al.* (1999) also found no role for RyRs in dendritic Ca^{2+} signalling. Thus, activation of extrasynaptic NMDARs by glutamate spillover during repetitive TBS could be well suited to regulating dendritic Ca^{2+} signals.

We also found that IP_3Rs do not contribute to dendritic Ca^{2+} transients until the second TBS is delivered. This could explain why LTP induced by 1 TBS is not dependent on IP_3R activation. A threshold level of synaptic

stimulation is required to trigger mGluR/IP_3-mediated dendritic Ca^{2+} transients (Nakamura *et al.* 1999; Zhou & Ross, 2002). This may reflect the need to generate sufficient levels of glutamate to activate perisynaptically located mGluRs (Lujan *et al.* 1996), or to produce spillover to activate extrasynaptic NMDARs (Lozovaya *et al.* 2004). In our experiments, the first TBS induces significant post-tetanic potentiation reflecting enhanced glutamate release for several minutes post-TBS. Thus, a second TBS delivered 30 s later would release significantly more glutamate. Alternatively, repeated tetanizations may be required to generate sufficient levels of IP_3 (Finch & Augustine, 1998).

We propose that IP_3R-mediated Ca^{2+} release is involved in activating local dendritic protein synthesis underlying LTP 2 (Fig. 8). Protein synthesis machinery and many different mRNAs are present in dendrites, mostly directly beneath synaptic sites (Steward & Schuman, 2001). Several examples of dendritic protein synthesis potentially modulated by Ca^{2+} have now been reported (reviewed by Kelleher *et al.* 2004*b*). Of particular interest is the ERK/MAPK signalling pathway (Kelleher *et al.* 2004*a*). Disruption of ERK activity caused a selective impairment in LTP 2 and prevented phosphorylation of key translational elements, including ribosomal protein S6 and eukaryotic initiation factor 4E (eIF4E). Importantly, these effects were also observed in synaptoneurosome preparations, indicating an important role for ERK signalling in local protein synthesis.

Somatic Ca^{2+} and LTP 3

The full expression of LTP 3 requires both L-VDCC and NMDAR activity. However, L-VDCC activity appears more important since nifedipine prevents LTP 3, whereas inhibition of NMDARs only results in a slight reduction. The strong effect of nifedipine on somatic Ca^{2+} suggests that repetitive increases in somatic Ca^{2+} via L-VDCCs triggers the gene transcription underlying the maintenance of LTP 3 (Fig. 8; Impey *et al.* 1996). However, we cannot rule out the possible involvement of a cumulative L-VDCC mediated spine signal in the induction of LTP 3. Inhibition of L-VDCCs also inhibits the early phase of LTP induced by 8 TBS (Fig. 2*E*), without affecting the early phases of LTP 1 or LTP 2. It may be that the cumulative effect of L-VDCC-mediated Ca^{2+} in the spine triggers an additional mechanism that contributes to the early phase of LTP induced by 8 TBS. The insensitivity of somatic Ca^{2+} to D-AP5 suggests that the small role of NMDARs in LTP 3 is due to Ca^{2+} signalling elsewhere in the neurone. It seems likely that this signal is reflected in the residual NMDAR-sensitive Ca^{2+} transient that we observed in spines and dendrites when stores were inhibited.

The transcription factor cyclic-AMP-responsive element-binding protein (CREB) is generally regarded as a key element in the maintenance of LTP 3 (West *et al.* 2002). CREB-dependent transcription requires both phosphorylation of CREB and recruitment of the coactivator CREB-binding protein (CBP). Although both L-VDCCs and NMDARs can lead to CREB phosphorylation, only L-type VDCCs produce the necessary signal to recruit CBP (Hardingham *et al.* 1999) and trigger CRE-mediated gene expression (Impey *et al.* 1996). Again, although by necessity we have analysed Ca^{2+} signals within a large compartment, a smaller microdomain involving a close association between L-VDCCs and calmodulin is likely to be important in this process (Deisseroth *et al.* 1998; Dolmetsch *et al.* 2001). The small role of NMDARs in LTP 3 may reflect a prolongation of CREB phosphorylation, increasing the time window for CREB–CBP interaction. On the other hand, NMDARs are very effective activators of serum-responsive element (SRE)-dependent transcription (Bading *et al.* 1993), which could work in parallel with L-VDCC-triggered CREB transcription (Davis *et al.* 2000) during the late maintenance phase of LTP 3.

Different forms of LTP at CA3–CA1 synapses

We have now extended our previous findings from field recordings (Raymond & Redman, 2002) to single CA1 pyramidal neurones, eliminating the possibility that different forms of LTP were maintained by different subpopulations of neurones. We show that LTP 1, 2 and 3 coexist in the same neurone, and probably at the same synaptic contacts.

How do different forms of LTP interact, if at all? The induction of LTP 3 by 8 TBS should also, *en route*, activate LTP 1 and LTP 2. Indeed, potentiation remaining after inhibition of L-VDCCs during 8 TBS, or of IP_3Rs during 4 TBS, is similar to LTP 2 and LTP 1, respectively, inferring that weaker forms underlie more persistent forms of LTP. Conversely, inhibition of RyRs has no observable effect on LTP induced by 4 TBS or 8 TBS, and inhibition of IP_3Rs does not visibly alter LTP 3. To explain this, we previously hypothesized (Raymond & Redman, 2002) that since both RyRs and IP_3Rs have bell-shaped Ca^{2+}-response curves (Bezprozvanny *et al.* 1991; Finch *et al.* 1991), they would be inhibited by repeated tetanization. However, we now show that the Ca^{2+} contributions via RyRs and IP_3Rs do not vary from the second to the eighth TBS train. It remains possible that the downstream effectors activated by each Ca^{2+} source are inhibited by induction of more persistent LTP. An alternative explanation is that weaker effector mechanisms remain active, but become redundant once effectors associated with more persistent LTP are activated. Identification of the various effector mechanisms associated with different forms of LTP will be important in answering these questions.

References

Abraham WC & Huggett A (1997). Induction and reversal of long-term potentiation by repeated high-frequency stimulation in rat hippocampal slices. *Hippocampus* **7**, 137–145.

Abraham WC & Otani S (1991). Macromolecules and the maintenance of long-term potentiation. In *Kindling and Synaptic Plasticity. The Legacy of Graham Goddard*, ed. Morrell F, pp. 92–109. Birkhauser, Boston.

Augustine GJ, Santamaria F & Tanaka K (2003). Local calcium signaling in neurons. *Neuron* **40**, 331–346.

Bading H, Ginty DD & Greenberg ME (1993). Regulation of gene expression in hippocampal neurons by distinct calcium signaling pathways. *Science* **260**, 181–186.

Bezprozvanny I, Watras J & Ehrlich BE (1991). Bell-shaped calcium-response curves of Ins (1,4,5), P3- and calcium-gated channels from endoplasmic reticulum of cerebellum. *Nature* **351**, 751–754.

Bliss TVP & Collingridge GL (1993). A synaptic model of memory: long-term potentiation in the hippocampus. *Nature* **361**, 31–39.

Bliss TV & Gardner-Medwin AR (1973). Long-lasting potentiation of synaptic transmission in the dentate area of the unanaesthetized rabbit following stimulation of the perforant path. *J Physiol* **232**, 357–374.

Christie BR, Eliot LS, Ito K, Miyakawa H & Johnston D (1995). Different Ca^{2+} channels in soma and dendrites of hippocampal pyramidal neurons mediate spike-induced Ca^{2+} influx. *J Neurophysiol* **73**, 2553–2557.

Cohen AS, Raymond CR & Abraham WC (1998). Priming of long-term potentiation induced by activation of metabotropic glutamate receptors coupled to phospholipase C. *Hippocampus* **8**, 160–170.

Davare MA, Avdonin V, Hall DD, Peden EM, Burette A, Weinberg RJ, Horne MC, Hoshi T & Hell JW (2001). A beta2 adrenergic receptor signaling complex assembled with the Ca^{2+} channel Cav1.2. *Science* **293**, 98–101.

Davis S, Vanhoutte P, Pages C, Caboche J & Laroche S (2000). The MAPK/ERK cascade targets both Elk-1 and cAMP response element-binding protein to control long-term potentiation-dependent gene expression in the dentate gyrus *in vivo*. *J Neurosci* **20**, 4563–4572.

De Koninck P & Schulman H (1998). Sensitivity of CaM kinase II to the frequency of Ca^{2+} oscillations. *Science* **279**, 227–230.

Deisseroth K, Heist EK & Tsien RW (1998). Translocation of calmodulin to the nucleus supports CREB phosphorylation in hippocampal neurons. *Nature* **392**, 198–202.

Delmas P & Brown DA (2002). Junctional signaling microdomains: bridging the gap between the neuronal cell surface and Ca^{2+} stores. *Neuron* **36**, 787–790.

Dolmetsch RE, Pajvani U, Fife K, Spotts JM & Greenberg ME (2001). Signaling to the nucleus by an L-type calcium channel–calmodulin complex through the MAP kinase pathway. *Science* **294**, 333–339.

Emptage N, Bliss TV & Fine A (1999). Single synaptic events evoke NMDA receptor-mediated release of calcium from internal stores in hippocampal dendritic spines. *Neuron* **22**, 115–124.

Feng W, Tu J, Yang T, Vernon PS, Allen PD, Worley PF & Pessah IN (2002). Homer regulates gain of ryanodine receptor type 1 channel complex. *J Biol Chem* **277**, 44722–44730.

Finch EA & Augustine GJ (1998). Local calcium signalling by inositol-1,4,5-trisphosphate in Purkinje cell dendrites. *Nature* **396**, 753–756.

Finch EA, Turner TJ & Goldin SM (1991). Calcium as a coagonist of inositol 1,4,5-trisphosphate-induced calcium release. *Science* **252**, 443–446.

Frey U, Frey S, Schollmeier F & Krug M (1996). Influence of actinomycin D, a RNA synthesis inhibitor, on long-term potentiation in rat hippocampal neurons *in vivo* and *in vitro*. *J Physiol* **490**, 703–711.

Gafni J, Munsch JA, Lam TH, Catlin MC, Costa LG, Molinski TF & Pessah IN (1997). Xestospongins: potent membrane permeable blockers of the inositol 1,4,5-trisphosphate receptor. *Neuron* **19**, 723–733.

Grover LM & Teyler TJ (1990). Two components of long-term potentiation induced by different patterns of afferent activation. *Nature* **347**, 477–479.

Hardingham GE, Chawla S, Cruzalegui FH & Bading H (1999). Control of recruitment and transcription-activating function of CBP determines gene regulation by NMDA receptors and L-type calcium channels. *Neuron* **22**, 789–798.

Hell JW, Westenbroek RE, Breeze LJ, Wang KK, Chavkin C & Catterall WA (1996). *N*-methyl-D-aspartate receptor-induced proteolytic conversion of postsynaptic class C L-type calcium channels in hippocampal neurons. *Proc Natl Acad Sci U S A* **93**, 3362–3367.

Huang YY & Kandel ER (1994). Recruitment of long-lasting and protein kinase A-dependent long-term potentiation in the CA1 region of hippocampus requires repeated tetanization. *Learn Mem* **1**, 74–82.

Impey S, Mark M, Villacres EC, Poser S, Chavkin C & Storm DR (1996). Induction of CRE-mediated gene expression by stimuli that generate long-lasting LTP in area CA1 of the hippocampus. *Neuron* **16**, 973–982.

Kelleher RJ 3rd, Govindarajan A, Jung HY, Kang H & Tonegawa S (2004*a*). Translational control by MAPK signaling in long-term synaptic plasticity and memory. *Cell* **116**, 467–479.

Kelleher RJ 3rd, Govindarajan A & Tonegawa S (2004*b*). Translational regulatory mechanisms in persistent forms of synaptic plasticity. *Neuron* **44**, 59–73.

Kennedy MB (2000). Signal-processing machines at the postsynaptic density. *Science* **290**, 750–754.

Lovinger DM, Wong KL, Murakami K & Routtenberg A (1987). Protein kinase C inhibitors eliminate hippocampal long-term potentiation. *Brain Res* **436**, 177–183.

Lozovaya NA, Grebenyuk SE, Tsinsadze TS, Feng B, Monaghan DT & Krishtal OA (2004). Extrasynaptic NR2B and NR2D subunits of NMDA receptors shape 'superslow' afterburst EPSC in rat hippocampus. *J Physiol* **558**, 451–463.

Lujan R, Nusser Z, Roberts JD, Shigemoto R & Somogyi P (1996). Perisynaptic location of metabotropic glutamate receptors mGluR1 and mGluR5 on dendrites and dendritic spines in the rat hippocampus. *Eur J Neurosci* **8**, 1488–1500.

Lynch MA (2004). Long-term potentiation and memory. *Physiol Rev* **84**, 87–136.

Magee JC & Johnston DJ (1995). Characterization of single voltage-activated Na^+ and Ca^{2+} channels in apical dendrites of rat CA1 pyramidal neurons. *J Physiol* **497**, 67–90.

Malinow R, Madison DV & Tsien RW (1988). Persistent protein kinase activity underlying long-term potentiation. *Nature* **335**, 820–824.

Martin SJ, Grimwood PD & Morris RG (2000). Synaptic plasticity and memory: an evaluation of the hypothesis. *Annu Rev Neurosci* **23**, 649–711.

Morgan SL & Teyler TJ (2001). Electrical stimuli patterned after the theta-rhythm induce multiple forms of LTP. *J Neurophysiol* **86**, 1289–1296.

Nakamura T, Barbara JG, Nakamura K & Ross WN (1999). Synergistic release of Ca^{2+} from IP_3-sensitive stores evoked by synaptic activation of mGluRs paired with backpropagating action potentials. *Neuron* **24**, 727–737.

Nakamura T, Lasser-Ross N, Nakamura K & Ross WN (2002). Spatial segregation and interaction of calcium signalling mechanisms in rat hippocampal CA1 pyramidal neurons. *J Physiol* **543**, 465–480.

Nakamura T, Nakamura K, Lasser-Ross N, Barbara JG, Sandler VM & Ross WN (2000). Inositol 1,4,5-trisphosphate (IP_3)-mediated Ca^{2+} release evoked by metabotropic agonists and backpropagating action potentials in hippocampal CA1 pyramidal neurons. *J Neurosci* **20**, 8365–8376.

Nguyen PV, Abel T & Kandel ER (1994). Requirement of a critical period of transcription for induction of a late phase of LTP. *Science* **265**, 1104–1107.

Otani S, Marshall CJ, Tate WP, Goddard GV & Abraham WC (1989). Maintenance of long-term potentiation in rat dentate gyrus requires protein synthesis but not messenger RNA synthesis immediately post-tetanization. *Neuroscience* **28**, 519–526.

Petrozzino JJ, Pozzo Miller LD & Connor JA (1995). Micromolar Ca^{2+} transients in dendritic spines of hippocampal pyramidal neurons in brain slice. *Neuron* **14**, 1223–1231.

Racine RJ, Milgram NW & Hafner S (1983). Long-term potentiation phenomena in the rat limbic forebrain. *Brain Res* **260**, 217–231.

Raymond CR & Redman SJ (2002). Different calcium sources are narrowly tuned to the induction of different forms of LTP. *J Neurophysiol* **88**, 249–255.

Raymond CR, Thompson VL, Tate WP & Abraham WC (2000). Metabotropic glutamate receptors trigger homosynaptic protein synthesis to prolong long-term potentiation. *J Neurosci* **20**, 969–976.

Sabatini BL, Maravall M & Svoboda K (2001). Ca^{2+} signaling in dendritic spines. *Curr Opin Neurobiol* **11**, 349–356.

Sabatini BL & Svoboda K (2000). Analysis of calcium channels in single spines using optical fluctuation analysis. *Nature* **408**, 589–593.

Sala C, Piech V, Wilson NR, Passafaro M, Liu G & Sheng M (2001). Regulation of dendritic spine morphology and synaptic function by Shank and Homer. *Neuron* **31**, 115–130.

Sharp AH, McPherson PS, Dawson TM, Aoki C, Campbell KP & Snyder SH (1993). Differential immunohistochemical localization of inositol 1,4,5-trisphosphate- and ryanodine-sensitive Ca^{2+} release channels in rat brain. *J Neurosci* **13**, 3051–3063.

Steward O & Schuman EM (2001). Protein synthesis at synaptic sites on dendrites. *Annu Rev Neurosci* **24**, 299–325.

Tu JC, Xiao B, Naisbitt S, Yuan JP, Petralia RS, Brakeman P, Doan A, Aakalu VK, Lanahan AA, Sheng M & Worley PF (1999). Coupling of mGluR/Homer and PSD-95 complexes by the Shank family of postsynaptic density proteins. *Neuron* **23**, 583–592.

West AE, Griffith EC & Greenberg ME (2002). Regulation of transcription factors by neuronal activity. *Nat Rev Neurosci* **3**, 921–931.

Westenbroek RE, Ahlijanian MK & Catterall WA (1990). Clustering of L-type Ca^{2+} channels at the base of major dendrites in hippocampal pyramidal neurons. *Nature* **347**, 281–284.

Yasuda R, Sabatini BL & Svoboda K (2003). Plasticity of calcium channels in dendritic spines. *Nat Neurosci* **6**, 948–955.

Zhou S & Ross WN (2002). Threshold conditions for synaptically evoking Ca^{2+} waves in hippocampal pyramidal neurons. *J Neurophysiol* **87**, 1799–1804.

Acknowledgements

The authors thank R. Tsien, G. Stuart and J. Bekkers for critical reading and advice. This work was supported by the National Health and Medical Research Council of Australia.